Journal of Applied Fluid Mechanics, Vol. 18, No. 6, pp. 1524-1533, 2025.
Available online at www.jafmonline.net, ISSN 1735-3572, EISSN 1735-3645.
https://doi.org/10.47176/jafm.18.6.3135

Influence of Clearances in Variable Guide Vanes and Stators on the Performance of a Multi-stage Compressor and Its Flow Control

L. Huang[1, 2†], W. Chu[1], H. Zhang[1] and Z. Guo[1,3]

[1] *School of Power and Energy, Northwestern Polytechnical University, Xi'an 710129, China*
[2] *AECC Sichuan Gas Turbine Establishment, Chengdu 610500, China*
[3] *Test Center, National University of Defense Technology, Xi'an 710106, China*

†*Corresponding Author Email: hjc666@mail.nwpu.edu.cn*

ABSTRACT

In pursuit of enhanced accuracy in the performance prediction and optimization of high-load compressors, this study emphasizes the significance of empirically measured clearance values associated with variable guide vanes and stators in engineering applications. Utilizing these empirical data, we conduct a refined modeling approach for the variable guide vanes and stators. A comprehensive three-dimensional numerical simulation methodology is employed to examine the impact and underlying flow mechanisms of the adjustable blades with clearances in a nine-stage compressor, concurrently optimizing the positional parameters of the clearances to augment the aerodynamic performance of the compressor. The findings of this investigation reveal that the omission of clearances and platform geometry of adjustable blades in numerical simulations can lead to an overestimation of both maximum flow rates and the overall stability margins. Driven by the pressure differential between the suction and pressure sides, clearance leakage flow is generated at the leading edge of the end wall of adjustable blades, exacerbating flow separation in the end wall corner region and potentially resulting in corner stall phenomena. By adjusting the platform of the adjustable stators, which experience corner stall predominantly, the leading edge separation resulting from the interaction of the flow near the end wall and the leakage flow from the leading edge clearance is mitigated. Consequently, the maximum flow rate of the compressor is increased by approximately 0.48 kg/s, the overall stability margin is enhanced by approximately 7.52%, and the peak efficiency experiences an improvement of about 0.4%.

Article History

Received September 16, 2024
Revised January 2, 2025
Accepted January 14, 2025
Available online March 30, 2025

Keywords:

Multi-stage compressor
Adjustable stator
Stator clearance
Clearance optimization
Aerodynamic stability

1. INTRODUCTION

As a fundamental element of aero-engines, the performance of axial compressors holds significant importance (Guo et al., 2022). Within the context of the radial clearance of compressor blades, a portion of the fluid, driven by pressure differentials, transitions from the pressure side to the suction side. This phenomenon results in clearance leakage flow, which is accompanied by associated losses. The leakage flow, influenced by both mainstream and secondary flows in proximity to the endwall, evolves downstream into clearance leakage vortices. These vortices contribute to blockage in the endwall region and exacerbate flow losses, thereby adversely impacting the overall aerodynamic performance of the compressor (Zhang et al., 2020a). Furthermore, as the compressor experiences increased throttling, clearance leakage flow emerges as a principal factor contributing to flow instability phenomena, such as rotating stall (Zhang et al., 2020b).

A substantial amount of research has been conducted on rotor tip clearance in compressors (Adamczyk et al., 1993; Baghdadi, 1996; Suder & Celestina, 1996; Zhang et al., 2023; Zheng & Yang, 2016; Lange et al., 2018; Cao & Zhai, 2019; Jiang et al., 2023), resulting in a wealth of findings. For instance, Adamczyk et al. (1993) conducted a comprehensive study on the flow effects of tip clearances in NASA Rotor 67, comparing the performance of the compressor across three distinct clearances. Their findings indicated that, as tip clearance increased, both the compressor pressure ratio and efficiency decreased, concomitantly leading to a reduction in the stable operating range. Baghdadi (1996) extensively explored the relationship

NOMENCLATURE

C_z	axial chord length	*Si*	guide vanes or stators
Ki	clearance of adjustable blades	SS	Suction Surface
p	pressure	VBC	Variable Blade Clearance
PS	pressure surface	V_z	axial velocity
q_{in}	dynamic pressure at blade inlet	WVBC	Without Variable Blade Clearance
Ri	rotors	ρ	density
SF	Stall Factor	Ψ	aerodynamic load coefficient

between clearance size and compressor surge margin, demonstrating that when the tip clearance is less than 1% of the chord length, variations in tip clearance exhibit minimal sensitivity regarding the stable operating range. However, as the clearance size increases, a linear relationship emerges between clearance size and the decrease in surge margin. Zheng and Yang (2016) examined the impact of clearance size on the performance of a 5-stage axial compressor, revealing that an increase in clearance from 0% to 5% of blade height correlates with a 21.8% reduction in blockage flow, a 43.1% decrease in maximum pressure ratio, and a 14.3% decline in maximum efficiency. Cao and Zhai (2019) employed numerical simulations to analyze the effects of clearance size on the performance of a high-pressure compressor in a civil high bypass ratio turbofan engine, finding that when clearance exceeds 0.3 mm, the increase in clearance size is approximately linearly related to the decrease in blockage flow.

Moreover, Pham et al. (2002) conducted numerical simulations on compressors of different stages and found that blade tip clearance had a greater impact on efficiency, but a relatively smaller impact on pressure ratio. Cheng et al. (2022) studied the effect of blade tip clearance variation on the aerodynamic performance of a 1.5-stage transonic compressor at different Reynolds numbers. Rannou et al. (2022) studied the significant effect of blade tip clearance variation on the performance of a single-stage compressor under near stall conditions.

The aforementioned literature indicates that the size of rotor tip clearance significantly impacts the efficiency and stability margin of compressors, a factor that warrants careful consideration. In the current design of high-load compressors, variable guide vanes and stators are employed to enhance both the efficiency and stability margin of the compressor under medium and low-speed conditions. This is achieved by modulating the stagger angle of the adjustable blades in correspondence with varying operational speeds. To prevent interference or flow stall due to the variable guide vanes and stators at different adjustment angles, a sufficiently large clearance with a platform is typically reserved, which varies in accordance with the adjustment angle. The clearance present before and after the platform of the variable guide vanes and stators inevitably gives rise to clearance leakage flow, thereby influencing the aerodynamic performance of the compressor. However, the majority of studies addressing radial clearances of compressor blades have primarily focused on rotor tip clearances and often neglect the clearances associated with adjustable blades. Consequently, investigating the impact of the clearances of variable guide vanes and stators on the performance of multi-stage compressors holds significant practical engineering relevance, particularly for achieving accurate performance predictions and refined flow field analyses of compressors. Furthermore, once the mechanisms by which the clearances of variable guide vanes and stators influence performance are elucidated, optimizing the configuration of these components can provide further guidance for improving the performance of high-load compressors.

Drawing upon actual measured clearance values preceding and succeeding the platform of the variable guide vanes and stators in engineering contexts, this paper undertakes a detailed modeling of the guide vanes and stators within the compressor. A fully three-dimensional numerical simulation is employed to investigate the influences and flow mechanisms associated with the applied clearances of the guide vanes and stators on the performance of a nine-stage compressor. Additionally, through the optimization of the platform position, enhancements in the overall aerodynamic performance of the compressor are anticipated.

2. RESEARCH OBJECT AND NUMERICAL SCHEMES

2.1 Research Object

The subject of this research paper is a 9-stage axial compressor. The inlet guide vane (S0) and the first three rows of stator blades (S1, S2, and S3) are designed to be adjustable. Table 1 provides the control rules for adjusting the stagger angles of S0 at varying rotational speeds, while the adjustment angles of the remaining stators are determined based on a specified proportion.

As illustrated in Fig. 1, the variable guide vanes and stators exhibit defined platforms and clearances. Specifically, K1 and K3 indicate the leading edge and trailing edge clearances, respectively, between the adjustable blades and the casing, while K2 and K4 denote the leading edge and trailing edge clearances between the adjustable blades and the hub. To prevent interference of the leading and trailing edges of the adjustable blades

Table 1 Control law of S0 at different speeds

Relative speed	Adjustment value（°）
1.0	0
0.85	−10
0.80	−15
0.741	−20
0.707	−20

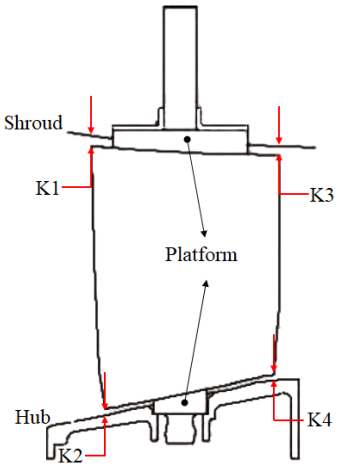

Fig. 1 Structural diagram of variable guide vanes and stators

Table 2 Clearance values for variable guide vanes and stators at 70.7% converted speed

Clearance	S0	S1	S2	S3
K1/mm	2.57	1.75	1.67	1.12
K2/mm	0.53	2.46	1.27	0.77
K3/mm	2.27	1.25	0.42	0.30
K4/mm	1.25	1.87	0.91	0.32

with the flow passage during significant angle adjustments, the structural design typically incorporates varying clearance values for the leading edge and trailing edge of the platform. This study concentrates on the operating condition corresponding to a conversion speed of 70.7%. At this conversion speed, the clearance values for the variable guide vanes and stators are presented in Table 2.

2.2 Numerical Schemes

The assumption of periodicity is applied to the blade passages, and the NUMECA/Autogrid5 module is utilized to generate a structured grid for a single passage. The primary passages of each blade row adopt an O4H grid topology, while a butterfly grid topology is employed for the gaps between the rotor blade tips and the adjustable blades. The total number of grid points for the single passage calculation of the nine-stage compressor is approximately 9.8 million, with grid refinement occurring near the wall surfaces. Figure 2 presents a partial view of the grid for the nine-stage compressor calculation domain, and Fig. 3 illustrates the hub and casing grids for the S1 gap.

The generated single passage grid is subsequently subjected to steady-state numerical simulations utilizing the NUMECA/FineTurbo module, with the Reynolds-Averaged Navier-Stokes equations and the Spalart–Allmaras turbulence model employed. This turbulence model has been widely recognized for its efficacy in performance calculations for multistage axial compressors (Teng et al., 2018; Chen et al., 2022; Guo et al., 2023). The inlet conditions are defined with axial inflow, total temperature (288.2 K), and total pressure (101325 Pa). The outlet conditions

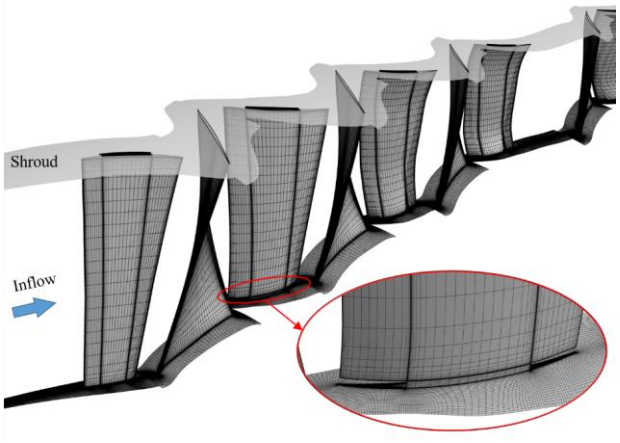

Fig. 2 Partial grid of computational domain

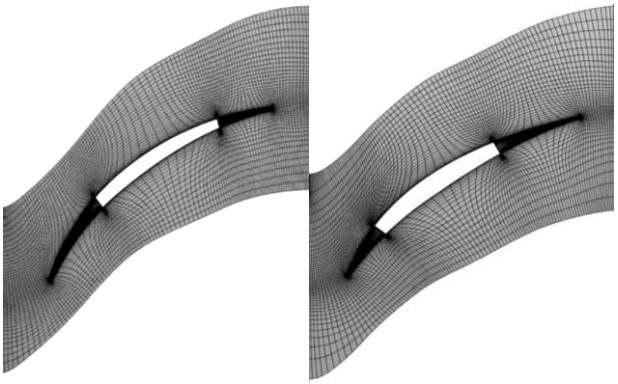

(a) Hub (b) Shroud

Fig. 3 Hub grid and shroud grid of S1 gap

are specified as average static pressure. The interface between the rotor and stator blades is managed using the mixing plane approach, which ensures strict conservation of mass, momentum, and energy at the interface. The wall surfaces are characterized as adiabatic and slip walls, encompassing the blade surfaces, hub, and casing. Among these wall surfaces, the casing remains stationary, while the blade surfaces and hub are in rotation. The flow on the solid walls adheres to the conditions of adiabatic flow and no-slip.

To validate the reliability of the aforementioned numerical approach, a comparison is conducted between the numerical results and experimental data at a conversion speed of 70.7%. The results reveal that the relative error between the maximum flow rate obtained from the numerical calculations and the experimental value is merely 0.21%. Similarly, the relative error for the near-stall flow rate is only 0.12%, and the relative error for the pressure ratio under near-stall conditions is approximately 4.63% when compared to the experimental values. These findings substantiate the reliability of the numerical approach employed in this study.

Moreover, a speed of 74.1% numerical model is used for validation. The peak efficiency was calculated using Spalart–Allmaras, k-epsilon (Extended Wall Function), k-epsilon (Low Re Yang Shih), and Shear Stress Transfer

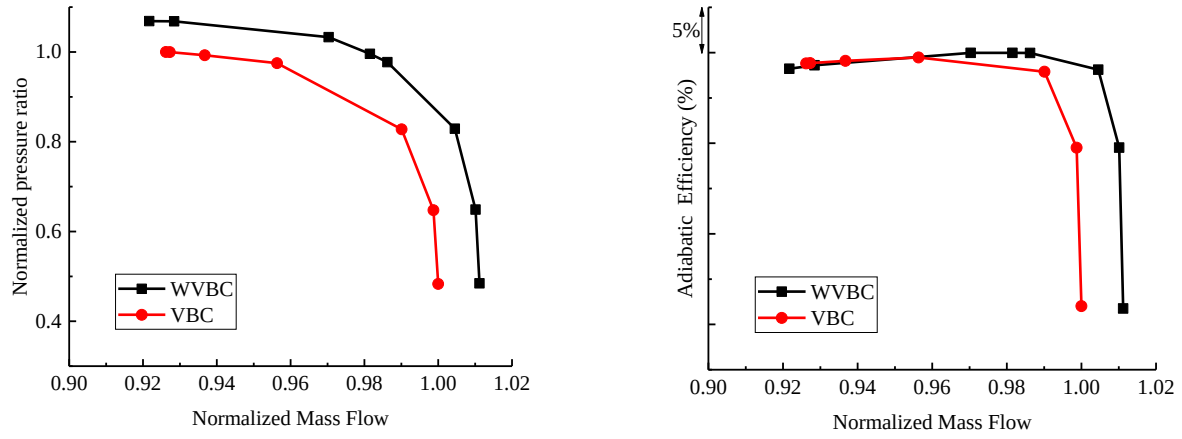

(a) Mass flow-Pressure ratio (b) Mass flow-Adiabatic efficiency

Fig. 4 Performance curves considering variable blade clearance

Table 3 Comparison between CFD results and experimental values under different turbulence models

Turbulence model	Peak efficiency
Spalart–Allmaras	86.45%
k-epsilon (Extended Wall Function)	88.37%
k-epsilon (Low Re Yang Shih)	87.90%
Shear Stress Transfer	87.81
Experiment value	86.5%

models. Table 3 shows the comparison between CFD results and experimental values under different turbulence models. From the table, it can be seen that the results calculated under the Spalart–Allmaras model are more consistent with the experimental values, further illustrating that the reliability of the numerical approach employed in this study.

3. IMPACT OF CLEARANCES IN VARIABLE GUIDE VANES AND STATORS ON PERFORMANCE OF MULTI-STAGE COMPRESSORS

3.1 Analyses of Overall Performance

To investigate the impact of clearances in variable guide vanes and stator blades on the performance of a nine-stage compressor, Fig. 4 presents the overall performance curve of the compressor. In this figure, WVBC (Without Variable Blade Clearance) denotes the compressor configuration without clearances in the variable guide vanes and stator blades, with parameters K1 = K3 = K4 = 0 mm. Conversely, VBC (Variable Blade Clearance) refers to the compressor configuration with specified clearances in the variable guide vanes and stators, as detailed in Table 2. The WVBC case utilizes the same grid and computational settings as the VBC case. Furthermore, the dimensionless flow rate depicted in the figure is normalized against the maximum flow rate of the VBC, while the dimensionless pressure ratio is normalized against the maximum pressure ratio of the VBC.

From Fig. 4, it is evident that, in comparison to WVBC, VBC exhibits significant alterations in maximum flow rate, near-stall flow rate, and pressure ratio, whereas the variations in peak efficiency are relatively minor. Calculations indicate that, relative to the WVBC configuration, the VBC configuration experiences a reduction of approximately 0.52 kg/s in maximum flow rate, a decrease of 6.88% in the comprehensive stability margin, and a reduction of 0.5% in peak efficiency. These findings suggest that the incorporation of adjustable designs in the guide vanes and stators of multistage axial compressors necessitates careful consideration of clearance and platform features during numerical simulations to accurately assess the overall performance of the compressor; otherwise, there exists a risk of overestimating both the maximum flow rate and the comprehensive stability margin.

3.2 Analyses of Flow Field

Based on the analysis presented in the preceding subsection, we have established that the comprehensive stability margin of the compressor significantly diminishes when accounting for clearance in the adjustable blades. Therefore, this subsection will concentrate on the analysis of the near-stall flow field to further investigate the flow mechanisms underlying the reduction in the comprehensive stability margin. To ensure a valid comparison between the near-stall flow fields, the flow fields for both WVBC and VBC have been selected at an equivalent flow rate.

Figure 5 illustrates the color contour of pitchwise-averaged dense flow (ρV_z, where ρ denotes fluid density and V_z denotes fluid axial velocity) for the compressor. From this figure, it can be observed that the introduction of clearances in the variable guide vanes and stators results in a shift in the location of instability within the compressor, transitioning from the blade tip of the first-stage rotor (R1) and the fourth-stage rotor (R4) to the blade tip of R1 and the root regions of the first and second-stage stators (S1 and S2). Consequently, the compromised flow at the root regions of S1 and S2 emerges as a crucial

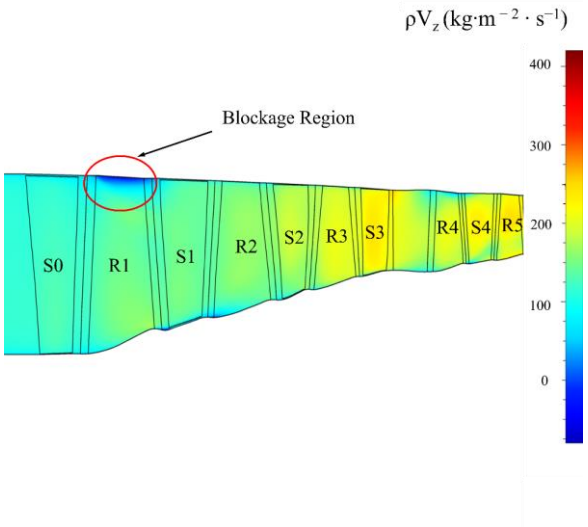

(a) WVBC

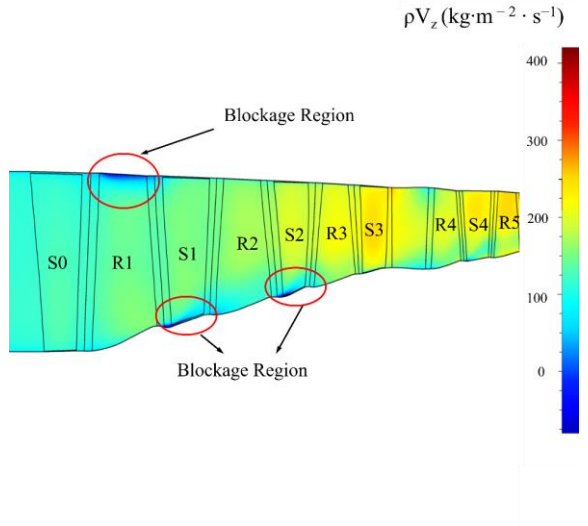

(b) VBC

Fig. 5 Contour of pitchwise-averaged dense flow

factor contributing to the diminished aerodynamic stability of the VBC configuration.

The analysis presented herein focuses on the flow dynamics at the root section of S1. Figure 6 illustrates the three-dimensional flow field in proximity to the root region of S1. In this figure, the red streamlines adjacent to the wall represent the limit streamlines, which elucidate the extent of corner separation, while the blue transparent iso-surface corresponds to the V_z = -0.1 m/s iso-surface, illustrating the accumulation of low-energy fluid in the corner region. From Fig. 6(a), it can be observed that for the WVBC, only a minimal volume of fluid accumulates in the corner region of the trailing edge after the upstream flow interacts with the leading edge of S1. Conversely, Fig. 6(b) indicates that, due to the proximity of the clearance platform to the mid-chord of the blade, a clearance leakage flow is generated at the leading edge clearance of S1 in the VBC scenario, driven by the pressure differential between the suction and pressure surfaces. This leakage flow circumvents the leading edges of the two rows of S1 and subsequently enters the S1 passage. Owing to the lower velocity of the leakage flow, it ultimately encounters

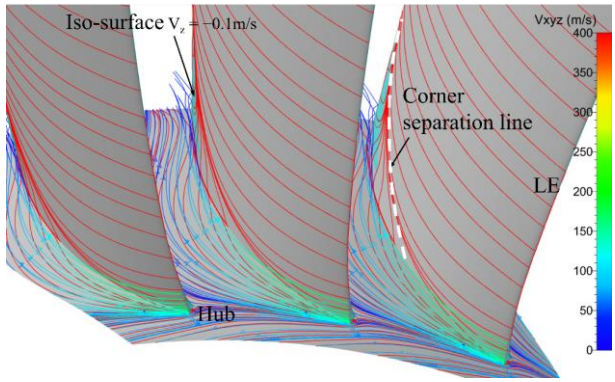

(a) WVBC

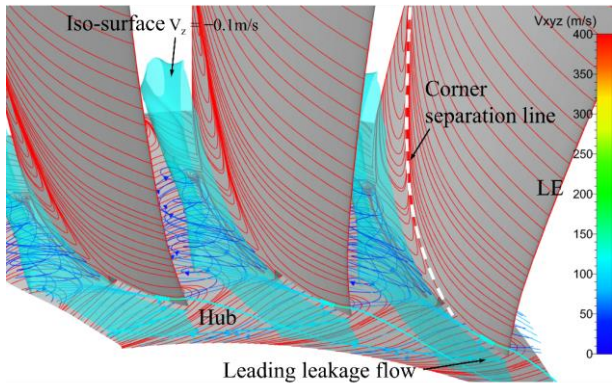

(b) VBC

Fig. 6 Three dimensional flow field near the S1 root

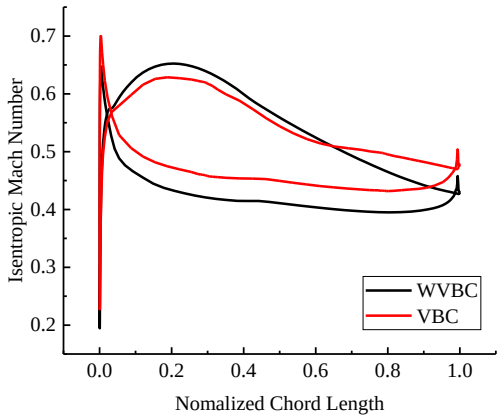

Fig. 7 Isentropic Mach number distribution on the S1 surface at 10% span

blockage and accumulation within the passage under the influence of adverse pressure gradients. This phenomenon significantly exacerbates the corner separation at the S1 root compared to the WVBC case.

Figure 7 displays the distribution of the isentropic Mach number at 10% span of S1. It is evident that, in comparison to the WVBC scenario, the aerodynamic load near the root of S1 in the VBC condition experiences a substantial decrease. This suggests that the expansion capability of the S1 root in response to airflow is diminished due to the enlarged corner separation. However, from both Fig. 6(b) and the outlet flow angle

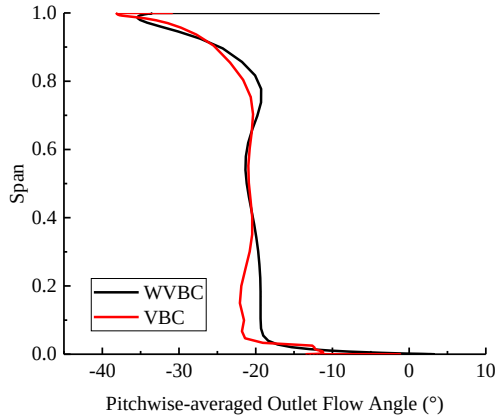

Fig. 8 Pitchwise-averaged outlet flow angle of S1 along span

distribution along the span as depicted in Fig. 8, it is evident that the flow blockage phenomenon near the S1 root in the VBC case is more pronounced. These observations indicate that the aerodynamic load near the S1 root increases significantly in the VBC condition compared to the WVBC condition.

The mechanism underlying the degradation of the flow near the S2 root in the VBC case parallels that observed at the S1 root under similar conditions and will not be elaborated further here. It too results from flow blockage induced by the leakage flow occurring at the leading edge clearance, which intensifies the flow separation in the corner region. Consequently, the aerodynamic load near the S2 root in the VBC condition also increases substantially.

To further quantify the extent of corner separation, this study utilizes the Stall Factor (SF) as proposed by Lei et al. (2008). This factor has been extensively applied in quantitative investigations of flow separation within the corner region (Li et al., 2014; Ma et al., 2017). The SF is defined as follows:

$$\begin{cases} \Psi_{0.5\text{span}} \left[\int_0^1 \dfrac{p_{\text{PS}}(z) - p_{\text{SS}}(z)}{q_{\text{in}}} \mathrm{d}\left(\dfrac{z}{C_z} \right) \right]_{x=0.5\text{span}} \\ \Psi_{0.1\text{span}} \left[\int_0^1 \dfrac{p_{\text{PS}}(z) - p_{\text{SS}}(z)}{q_{\text{in}}} \mathrm{d}\left(\dfrac{z}{C_z} \right) \right]_{x=0.1\text{span}} \\ SF = \Psi_{0.5\text{span}} - \Psi_{0.1\text{span}} \end{cases} \tag{1}$$

Where Ψ represents the aerodynamic load coefficient, C_z denotes the axial chord length, q_{in} represents the dynamic pressure at the blade inlet, $p(z)$ represents the static pressure at the axial coordinate z on the blade surface, and x is the coordinate in the blade height direction. The subscripts SS and PS correspond to the suction and pressure sides of the blade, respectively. According to reference [15], a corner stall occurs on the blade when $SF > 0.16$. Table 4 presents a comparison of the stall factors of S1 and S2 at the root for WVBC and VBC. As seen, the corner stall occurs at the S1 and S2 roots only in VBC.

Table 4 Corner stall factor *SF* for S1 and S2

Scheme	S1	S2
WVBC	0.0851	0.0810
VBC	0.1809	0.1650

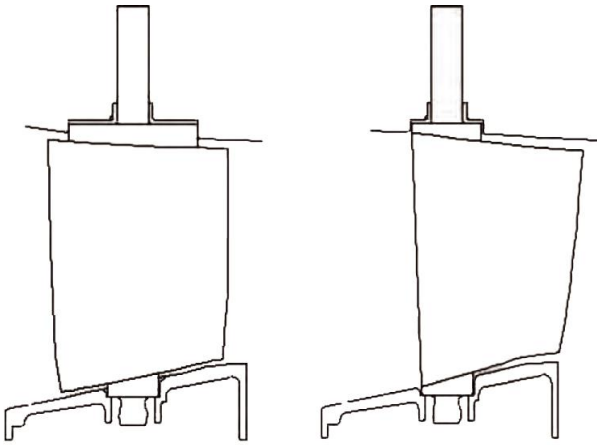

(a) Original S1 (b) Improved S1

Fig. 9 S1 clearances for two design concepts

Based on the preceding analysis, the underlying mechanism responsible for the reduced aerodynamic stability of VBC, in comparison to WVBC, can be articulated as follows: Under the pressure differential between the suction and pressure sides, a leakage flow develops at the leading edge clearances of S1 and S2 in VBC. This flow encounters blockage and accumulation within the passage, exacerbating flow separation and resulting in stall in the corner region. Consequently, the aerodynamic load at the root of S1 and S2 increases. This amplification in load on the preceding stages of the nine-stage compressor renders it more susceptible to instability.

4. OPTIMIZATION DESIGN OF ADJUSTABLE STATOR CLEARANCE

4.1 Clearance Optimization Design Scheme

The analysis presented in Section 3.2 indicates that the leading edge leakage flow at the root of the adjustable stator can precipitate corner stall. In pursuit of enhancing compressor performance, this study undertook an optimization design for the adjustable stator S1. Figure 9 provides a schematic representation of the improved design for S1. As illustrated in Fig. 9(b), the enhanced design incorporates the forward movement of the conical collar (adjusting axis). In this configuration, K1 = K2 = 0 mm, K3 = 1.25 mm, and K4 = 1.87 mm, signifying that the trailing edge clearance remains consistent with the original design. Figure 10 contrasts the original mesh with the mesh at the root clearance of S1, reflecting the forward movement of the conical collar.

4.2 Analyses of Overall Performance

To examine the effect of the improved S1 on the performance of the nine-stage compressor, Fig. 11 compares the overall performance curves of the

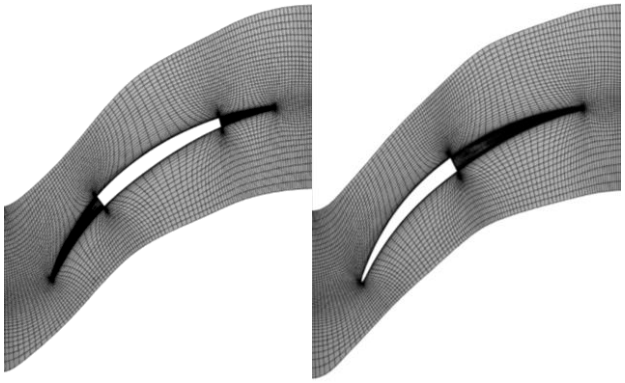

(a) Original S1 (b) Improved S1

Fig. 10 Root meshing of S1 comparison between two concepts

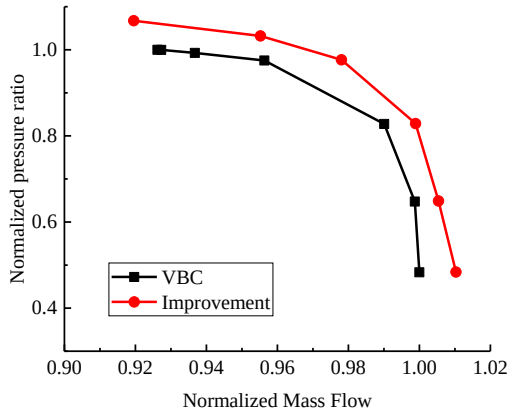

(a) Mass flow-Pressure ratio

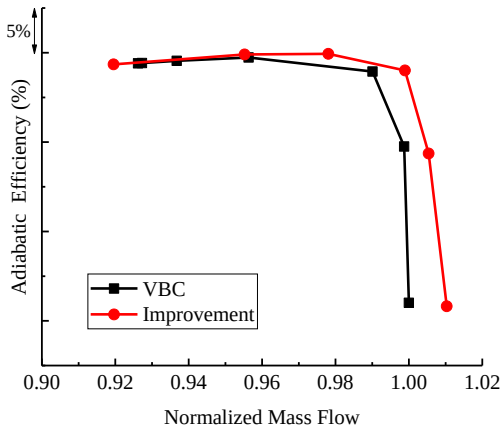

(b) Mass flow-Adiabatic efficiency

Fig. 11 Comparison of performance characteristics between VBC and Improvement

compressor before and after the enhancement. In this figure, "Improvement" denotes the compressor following the optimized design of the adjustable stator S1. The same mesh and computational settings as outlined in Section 2 were employed for the calculations pertaining to the "Improvement" case. Furthermore, the non-dimensional flow rate in the figure is normalized by the maximum flow

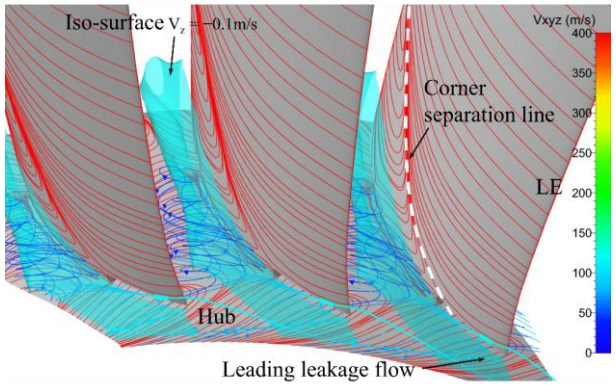

(a) VBC

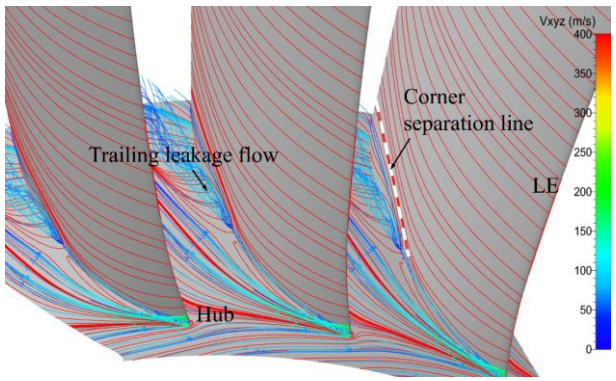

(b) Improvement

Fig. 12 Three dimensional flow field near S1 root

rate of VBC, while the non-dimensional pressure ratio is normalized by the maximum pressure ratio of VBC.

From Fig. 11, it can be observed that compared to the baseline case (VBC), the "Improvement" scenario exhibits significant enhancements in maximum flow rate, near-stall flow rate, and pressure ratio, while the increase in peak efficiency is relatively modest. Calculations indicate that the maximum flow rate of the "Improvement" case increases by approximately 0.48 kg/s, the comprehensive stability margin improves by approximately 7.52%, and the peak efficiency rises by approximately 0.4% relative to VBC.

4.3 Analyses of Flow Field

Based on the analysis presented in the previous subsection, the following conclusions can be drawn: The improved design for S1 markedly enhances the aerodynamic stability of the nine-stage compressor without compromising efficiency or maximum flow rate. Consequently, the near-stall flow field is selected for further analysis to elucidate the flow field mechanisms contributing to the improved aerodynamic stability of the compressor resulting from the modifications to S1. To ensure a fair comparison of the near-stall flow fields, the flow fields of VBC and Improvement were analyzed at an equivalent flow rate.

Consistent with the focus of Section 3.2, this subsection also emphasizes the flow dynamics near the root of S1. Figure 12 illustrates a comparison of the three-dimensional flow fields near the S1 root between VBC and

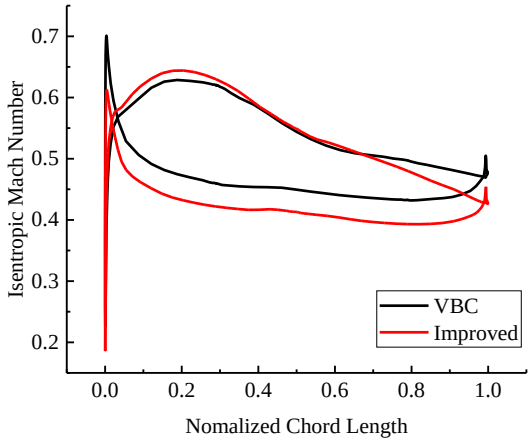

Fig. 13 Isentropic Mach number distribution on S1 surface at 10% span

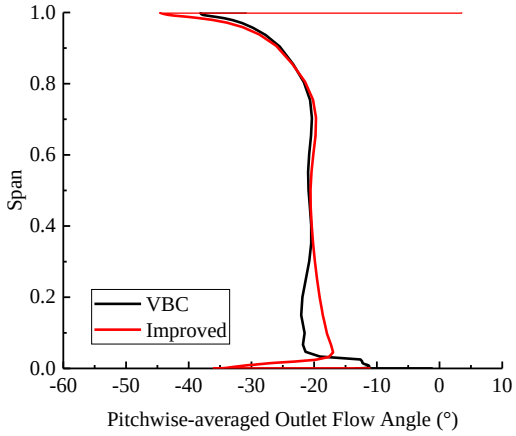

Fig. 14 Pitchwise-averaged outlet flow angle of S1 along span

Improvement. The red streamlines near the wall signify the limit streamlines, visualizing the extent of corner separation, while the blue transparent iso-surface represents the $V_z = -0.1$ m/s iso-surface, which depicts the accumulation of low-energy fluid in the corner region. It is evident that, in the VBC scenario, the position of the conical collar is situated closer to the midpoint of the blade, and the leakage flow emanating from the leading edge clearance obstructs the passage near the stator root, leading to large-scale flow separation in the corner region. In contrast, in the Improvement case, the forward displacement of the conical collar effectively mitigates the occurrence of flow blockage, which is caused by the interaction between the end wall flow and the leakage flow from the leading edge clearance, thereby making large-scale separation in the corner region less likely. Moreover, under the pressure differential between the suction and pressure sides, the leakage flow from the trailing edge clearance replenishes the low-speed fluid in the corner region of the stator with added momentum for downstream progression. This dynamic hinders the accumulation of the incoming flow in the corner region following the passage of the leading edge, further impeding the development of flow separation.

Furthermore, Fig. 13 compares the distribution of the isentropic Mach number at 10% span of S1 between the baseline configuration (VBC) and the improved design (Improvement). It is observed that, in comparison to VBC, Improvement exhibits a significant increase in aerodynamic load near the root of S1, indicating an enhanced ability of the stator root to diffuse the flow due to the reduction in corner separation. Figure 14 compares the distribution of the flow angle at the S1 outlet along the span between VBC and Improvement, revealing that the flow blockage near the S1 root is significantly diminished in Improvement. Through the analysis of Figs. 13 and 14, it can be concluded that the aerodynamic load near the S1 root is substantially reduced in Improvement.

Table 5 compares the stall factor *SF* at the roots of S1 and S2 between VBC and Improvement. It can be observed that following the implementation of the

Table 5 Corner stall factor *SF* for S1 and S2

Scheme	S1	S2
VBC	0.1809	0.1650
Improvement	0.0796	0.0824

improved S1, corner stall is suppressed in both S1 and S2. The mechanism underlying the improvement in flow near the root of S2 in Improvement can be readily explained. From Figs. 12 and 14, it is evident that the flow blockage in the S1 passage is alleviated with the improved S1, resulting in a reduction in the flow angle at the S1 outlet near the root. In a multi-stage axial compressor, changes in flow angle propagate downstream. Therefore, the reduction in the outlet flow angle at the S1 root will lead to a decrease in the inlet flow angle near the root of S2. Consequently, for Improvement, the strength of the leakage flow from the leading edge clearance at the root of S2 is weakened, leading to a relief in flow blockage within the S2 passage and a reduction in the severity of flow separation in the corner region, thus reducing the aerodynamic load. The pitch-wise averaged dense flow contour depicted in Fig. 15 further corroborates the aforementioned mechanism. As illustrated, with the implementation of the improved S1, the instability region of the compressor shifts from the blade tip of R1 and the roots of S1 and S2 to the blade tip of R1.

In summary, the mechanisms within the flow field that enhance the aerodynamic stability of the compressor through the refined design of the adjustable stator S1 can be delineated as follows: Firstly, the forward movement of the clearance platform in S1 mitigates the flow separation induced by the coupling effect between the endwall flow and the leakage flow from the leading edge clearance. Concurrently, the leakage flow emerging from the trailing edge clearance of S1 serves to augment the low-velocity fluid within the corner region, thereby further suppressing the progression of corner separation. Subsequently, the alleviation of flow blockage near the root of S1 leads to a reduction in the inlet flow angle adjacent to the root of S2. This trajectory results in a decrease in the intensity of the leakage flow through the leading edge clearance of S2,

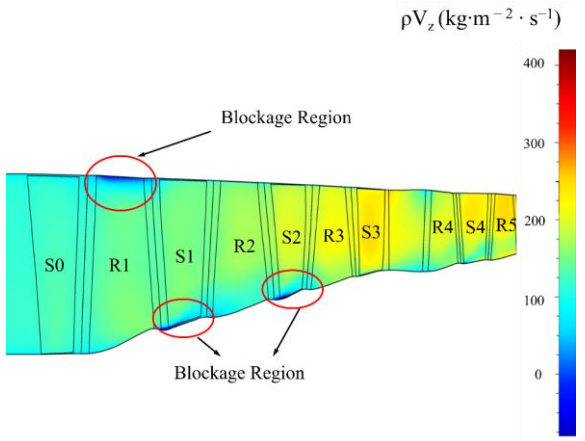

(a) VBC

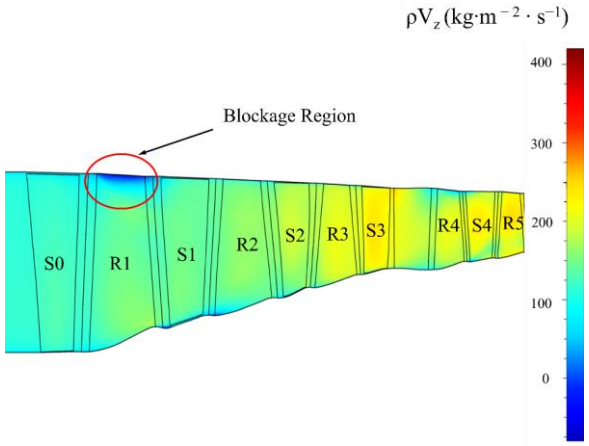

(b) Improvement

Fig. 15 Contour of pitch-wise averaged dense flow

thereby alleviating flow blockage and diminishing the severity of flow separation within the passage near the root of S2. Ultimately, the concurrent reduction in aerodynamic load near the roots of both S1 and S2 contributes to the enhancement of the compressor's aerodynamic stability.

5. CONCLUSION

This study employs a fully three-dimensional numerical simulation to examine the effects and flow mechanisms of variable guide vanes and stators, incorporating platforms and clearances, on the performance of a nine-stage compressor. Additionally, the optimization of the platform position is undertaken to enhance the overall aerodynamic performance of the compressor. The principal conclusions are as follows:

1. In the design of variable guide vanes and stators for a multi-stage axial compressor, it is imperative to consider the clearances and their platforms in numerical simulations to achieve a more precise evaluation of the compressor's overall performance. The omission of these factors may result in an overestimation of the maximum flow rate and the comprehensive stability margin.

2. By relocating the platform of the adjustable stator that experiences the earliest manifestation of corner separation, the maximum flow rate of the nine-stage compressor is increased by approximately 0.48 kg/s, the comprehensive stability margin is enhanced by about 7.52%, and the peak efficiency is improved by around 0.4%.

3. The presence of a pressure differential between the suction and pressure surfaces leads to the occurrence of leakage flow at the leading edge of the adjustable stator's end wall, resulting in blockage and accumulation within the passage. This condition exacerbates corner separation and may even precipitate corner stall.

4. Adjusting the platform position of the adjustable blades can suppress corner separation induced by the coupling effect between the endwall flow and the leakage flow through the leading edge clearance. Simultaneously, the leakage flow from the trailing edge clearance can provide low-energy fluid within the corner region, further inhibiting the evolution of corner separation.

ACKNOWLEDGEMENTS

Research funding: The authors thank for the support of National Natural Science Foundation of China (52076179).

CONFLICT OF INTEREST

The authors declare that they have no known competing financial interests or personal relationships that could have appeared to influence the work reported in this paper

AUTHORS CONTRIBUTION

L. Huang: Conceptualization, Data curation, Formal analysis, Funding acquisition, Investigation, Methodology, Software, Supervision, Validation, Visualization, Writing – original draft. **W. Chu:** Writing – review & editing, Supervision, Resources, Project administration. **H. Zhang:** Writing – review & editing, Validation, Project administration. **Z. Guo:** Methodology, Conceptualization.

REFERENCES

Adamczyk, J. J., Celestina, M. L., & Greitzer E. M. (1993). The role of tip clearance in high-speed fan stall. *Journal of Turbomachinery*, *155*(1), 28-39. https://doi.org/10.1115/1.2929212

Baghdadi, S. (1996). Modeling tip clearance effects in multistage axial compressors. *Journal of Turbomachinery*, *118*(4), 697-705. https://doi.org/10.1115/1.2840925

Cao, C., & Zhai, Z. (2019). Influence of tip clearance on civil high-bypass-ratio transonic compressor

aerodynamic performance. *Science Technology and Engineering*, *19*(10), 230-236. http://stae.com.cn/jsygc/article/abstract/1809897?st=search

Chen, Y., Gao, C., & Chu, W. (2022). Effect and mechanism of roughness on the performance of a five-stage axial flow compressor. *Aerospace*, *9*(8), 428. https://doi.org/10.3390/aerospace9080428

Cheng, H., Lu, X., Zhao, S, Huang, S., & Zhu, J. (2022). Effect of tip clearance variation in the transonic axial compressor of a miniature gas turbine at different Reynolds numbers. *Aerospace Science and Technology*, *128*, 107793. https://doi.org/10.1016/j.ast.2022.107793

Guo, Z., Chu, W., Yan, S., Shen, Z., & Wang, G. (2022). Data mining on effects of manufacturing error on aerodynamic performance and stability of compressor cascade. *Journal of Propulsion Technology*, *43*(3), 200576. https://doi.org/10.13675/j.cnki.tjjs.200576

Guo, Z., Chu, W., Zhang, H., Liang, C., & Meng, D. (2023). Statistical evaluation of stability margin of a multi-stage compressor with geometric variability using adaptive polynomial chaos-Kriging model. *Physics of Fluids*, *35*(7), 076114. https://doi.org/10.1063/5.0158821

Jiang, C., Wang, Z., Le, Z., & Hu, J. (2023). Numerical simulation of the effect of circumferential non-uniform tip clearance on rotating instability in a rotor. *Journal of Aerospace Power*. https://doi.org/10.13224/j.cnki.jasp.20220973

Lange, M., Rolfes, M., Mailach, R., & Schrapp, H. (2018). Periodic unsteady tip clearance vortex development in low-speed axial research compressor at different tip clearances. *Journal of Turbomachinery*, *140*(3), 031005. https://doi.org/10.1115/1.4038319

Lei, V. M., Spakovszky, Z. S., & Greitzer, E. M. (2008). A Criterion for axial compressor hub-corner stall. *Journal of Turbomachinery*, *130*(3), 031006. https://doi.org/10.1115/1.2775492

Li, X., Chu, W., & Zhang, H. (2014). Investigation on relation between secondary flow and loss on a high loaded axial-flow compressor cascade. *Journal of Propulsion Technology*, *35*(7), 914-925. https://doi.org/10.13675/j.cnki.tjjs.2014.07.007

Ma, S., Chu, W., Zhang, H., Kuang, H., & Li, X. (2017). Numerical investigation on secondary flow control in cascade with micro-vortex generator. *Journal of Propulsion Technology*, *38*(12), 2641-2651. https://doi.org/10.13675/j.cnki.tjjs.2017.12.001

Pham, H., Singh, A., Caillat J. (2002). Adaptive control for a refrigeration system using pulse width modulated duty cycle scroll compressor. America Patent: US20020178737A1, 2002-12-05.

Rannou, C., Dazin, A., Marty, J., Tanguy, G., Castillon, L., & Moubogha, J. (2022). *Effect of the axial compressor tip clearance size: performance and transition to rotating stall.* ASME Turbo Expo 2018: Turbomachinery Technical Conference and Exposition, No. GT2022-80914. American Society of Mechanical Engineers, 2022. https://doi.org/10.1115/GT2022-80914

Suder, K. L., & Celestina, M. L. (1996). Experimental and computational investigation of the tip clearance flow in a transonic axial compressor rotor. *Journal of Turbomachinery*, *118*(2), 218-229. https://doi.org/10.1115/1.2836629

Teng, X., Chu, W., & Zhang, H. (2018). *The influence of geometry deformation on a multistage compressor*. ASME Turbo Expo 2018: Turbomachinery Technical Conference and Exposition, No. GT2018-75935. American Society of Mechanical Engineers, 2018. https://doi.org/10.1115/GT2018-75935

Zhang, B., Liu, B., & Wang, H. (2020a). Impact of incidence angle on tip leakage flow control by endwall suction in a compressor cascade. *Journal of Aerospace Power*, *35*(11), 2400-2412. https://doi.org/10.13224/j.cnki.jasp.2020.11.017

Zhang, B., Liu, B., & Zhao, H. (2020b). Effects of blade tip suction on cascade gap leakage flow. *Journal of Propulsion Technology*, *41*(8), 1701-1709. https://doi.org/10.13675/j.cnki.tjjs.190585

Zhang, C., Zhang, G. Xu Z., Sun, D., & Liu, P. (2023). Analysis of effect mechanism of rotor tip clearance shapes on transonic axial compressor. *Aeroengine*, *49*(3), 66-74. https://doi.org/10.13477/j.cnki.aeroengine.2023.03.009

Zheng, X., & Yang, H. (2016). *Influence of tip clearance on the performance and matching of multistage axial compressors.* SME Turbo Expo 2016: Turbomachinery Technical Conference and Exposition, pages V02AT37A008- V02AT37A008. American Society of Mechanical Engineers, 2016. https://doi.org/10.1115/GT2016-56232